Spin-orbit relaxation and recombination dynamics in $I_2^-(CO_2)_n$ and $I_2^-(OCS)_n$ cluster ions: A new type of photofragment caging reaction

Andrei Sanov, Todd Sanford, Sreela Nandi, and W. Carl Lineberger
JILA, National Institute of Standards and Technology and University of Colorado, and Department of Chemistry and Biochemistry, University of Colorado, Boulder, Colorado 80309-0440

(Received 15 February 1999; accepted 16 April 1999)

We report a new type of photofragment caging reaction that is only possible because of the strong solvent-induced perturbation of the inherent electronic structure of the chromophore. The photoexcitation of I_2^- at 395 nm promotes it to a dissociative state correlating with $I^-+I^*(^2P_{1/2})$, the only near-ultraviolet dissociation channel for unsolvated I_2^-. In $I_2^-(CO_2)_n$ and $I_2^-(OCS)_n$ clusters, interaction with the solvent is observed to result in extremely fast spin-orbit relaxation. In general, we detect three reaction pathways: (1) direct dissociation of the chromophore to $I^-+I^*(^2P_{1/2})$; (2) the $I_2^-\rightarrow I^-+I^*$ dissociation, followed by spin-orbit quenching leading to $I^-+I(^2P_{3/2})$ products; and (3) the $I_2^-\rightarrow I^-+I^*$ dissociation, followed by spin-orbit quenching and $I^-+I(^2P_{3/2})\rightarrow I_2^-$ recombination and vibrational relaxation. We present experimental evidence of the spin-orbit relaxation and caging and discuss possible mechanisms. The results include: the measured translational energy release in 395 nm photodissociation of unsolvated I_2^-, indicating that solvation-free dissociation proceeds exclusively via the I^-+I^* channel; ionic product distributions in the photodissociation of size-selected $I_2^-(CO_2)_n$ and $I_2^-(OCS)_n$ clusters at the same wavelength, indicating the above three reaction channels; and ultrafast pump-probe measurements of absorption recovery, indicating picosecond time scales of the caging reaction. We rule out the mechanisms of spin-orbit quenching relying on I*-solvent interactions without explicitly considering the perturbed electronic structure of I_2^-. Instead, as described by Delaney *et al.* (companion paper), the spin-orbit relaxation occurs by electron transfer from I^- to $I^*(^2P_{1/2})$, giving $I(^2P_{3/2})+I^-$. The 0.93 eV gap between the initial and final states in this transition is bridged by differential solvation due to solvent asymmetry. Favorable comparison of our experimental results and the theoretical simulations of Delaney *et al.* yield confidence in the mechanism and provide understanding of the role of cluster structure in spin-orbit relaxation and recombination dynamics. © *1999 American Institute of Physics.* [S0021-9606(99)01726-2]

I. INTRODUCTION

The multitude of interactions implicated in solvation affords chemical reactions a variety of pathways and mechanisms. For decades, many experimental and theoretical studies have been directed at understanding the detailed mechanisms of reactions in solutions. Nonetheless, new effects and mechanisms continue to be discovered. Gas phase clusters are especially appealing for the studies of solvation; they serve as model microsolutions that simplify interpretation of observables and allow for unraveling the effects of solvation on a microscopic level.[1–4]

The effect of solvation can be described as threefold. The first and most obvious effect is the limitation of space available to the solute, whose motion becomes constrained by physical barriers. Second, the solvent acts as an energy bath, opening a pathway for internal relaxation of the solute. The third, and most theoretically challenging aspect of solvation, is the perturbation of the internal electronic structure of both the solute and the solvent.

This publication presents new experimental evidence for the paramount importance of solvent-induced perturbation of the electronic structure in driving the chemical reactions. This aspect of solvation is particularly critical for reactions involving nonadiabatic transitions between electronic states. It is especially important in clusters with weakly bound ionic cores, in which the strong ion-solvent interactions can be comparable to chemical bonding. For example, I_2^-, one of the most studied ionic chromophores,[5–42] has a dissociation energy of 1.01 eV,[43,44] compared to a typical solvent binding energy of ~0.2 eV per solvent molecule.[5,10] Clearly, the solvent-induced perturbation of the electronic structure cannot be considered trivial even in a moderate-size cluster.

Although solvent-induced perturbation of the solute electronic structure is always crucial for accurate modeling, different types of solvent-driven reactions require various degrees of such perturbation. In many cases, the perturbation is large, but the reaction could proceed, in principle, even if it were minimal. One example is solvent-induced recombination, or caging, of photofragments.[5–19,38–42,45–60] The fundamental appeal of this process is that it involves both the breaking and remaking of chemical bonds affected by solvation. The I_2^- caging reactions studied so far[5–20] evolved on potential energy surfaces correlating with the $I(^2P_{3/2})+I^-(^1S)$ dissociation limit (see I_2^- potentials in Fig. 1). With I_2^- dissociated via the visible/near-infrared (IR) transition (indicated by the shorter arrow in Fig. 1), the $I(^2P_{3/2})$

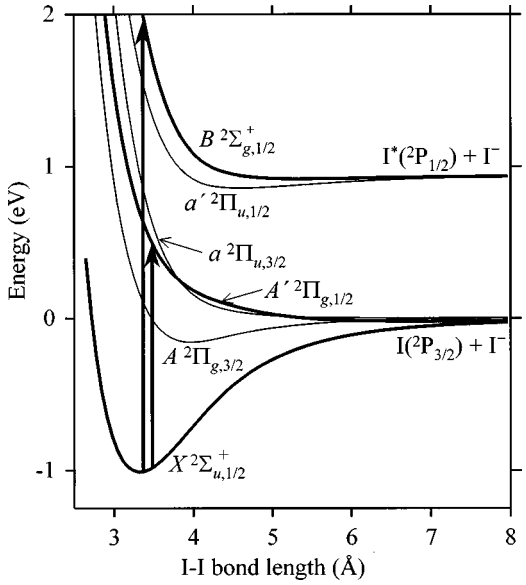

FIG. 1. The potentials of I_2^- calculated by Faeder *et al.* (Ref. 35), scaled to the experimental I_2^- well depth (Refs. 13 and 44). Arrows indicate the 790 and 395 nm transitions.

$+I^-(^1S)$ recombination proceeds via the mechanism[61–63] common for caging phenomena in both neutral and ionic, gas- and condensed phase systems. According to this mechanism, the fragment separation is halted by the solvent that absorbs the translational energy. The fragments recombine following the conversion at large separation to the ground I_2^- electronic state. Subsequently, the recombined I_2^- undergoes vibrational relaxation as the excitation energy is transferred to the solvent. Although the I_2^- electronic structure can be greatly perturbed by solvation,[37,64] only modest solvent-induced coupling between electronic states is actually needed, because the states in question are asymptotically degenerate.

In other cases, however, a much larger degree of solvent-induced perturbation of the inherent electronic structure of the solute is required for the reaction to be possible in principle. In a recent publication,[16] we presented first experimental evidence of a new type of caging reaction in which the I_2^- chromophore was dissociated within OCS clusters via the 395 nm transition indicated by the longer arrow in Fig. 1. The excitation leads to dissociation via the $I^*(^2P_{1/2}) + I^-(^1S)$ channel, where a simple reversal of fragment trajectories cannot result in recombination, because the $I^*(^2P_{1/2}) + I^-(^1S)$ potentials are not bound. [Hereinafter, I* denotes $I(^2P_{1/2})$.] Nevertheless, caging on the ground electronic state is observed, which requires electronic quenching of I* to precede the recombination. This crucial transition involves an energy mismatch of nearly 1 eV and is known to be extremely slow when occurring via radiative or collisional energy transfer mechanisms.

This paper and its companion[65] demonstrate that the observed spin-orbit quenching followed by I_2^- recombination is only possible because of the strong perturbation of I_2^- electronic structure by the solvent. We report further experimental evidence of this reaction and discuss possible mechanisms. In Sec. III, we first present the results showing that 395 nm photodissociation of unsolvated I_2^- proceeds exclusively via the $I^- + I^*$ channel, with no $I(^2P_{1/2} \rightarrow {}^2P_{3/2})$ relaxation. This observation proves that the spin-orbit relaxation of I* in clusters is driven by the solvent. We then report the ion product distributions in the photodissociation of $I_2^-(CO_2)_n$ and $I_2^-(OCS)_n$ clusters at the same wavelength. These distributions show that solvent-induced relaxation of the nascent photofragments leads to the formation of neutral I fragments in both spin-orbit states, and the spin-orbit relaxation is often followed by $I^- + I(^2P_{3/2}) \rightarrow I_2^-$ recombination. Finally, we present the ultrafast pump-probe measurements, which indicate a surprisingly fast (picosecond) rate of the caging reaction. In Sec. IV, we rule out the mechanisms that would explain the observed spin-orbit quenching without explicitly considering the perturbed I_2^- potentials. We then use the solvent asymmetry mediated electron transfer model, first suggested by Maslen *et al.*[37] and discussed in detail in the companion paper,[65] to interpret the experimental results. Favorable comparison of the experimental and calculated[65] results yields confidence in the proposed mechanism and allows for improved understanding of quenching dynamics.

The following chart describes the reaction steps and defines the final product channels as they are labeled throughout the paper:

$$I_2^- + 395\ \text{nm} \rightarrow I^*(^2P_{1/2}) + I^-(^1S) \rightarrow \text{final uncaged (type A) products} \quad \text{(A)}$$

$$\downarrow \text{spin-orbit quenching}$$

$$I(^2P_{3/2}) + I^-(^1S) \rightarrow \text{final uncaged (type B) products} \quad \text{(B)}$$

$$\downarrow \text{recombination}$$

$$I_2^- \rightarrow \text{final caged products} \quad \text{(C)}$$

As usual,[5–16] we refer to the $I_2^-(CO_2)_k$ and $I_2^-(OCS)_k$ fragments (channel C) as caged and the $I^-(CO_2)_k$ and $I^-(OCS)_k$ fragments as uncaged. In contrast to the previous studies, there are two classes of uncaged fragments in this caging reaction (channels A and B). Elsewhere, the terms ''caging'' and ''recombination'' are often used interchangeably to describe the caging reactions not involving spin-orbit quenching. Here, we distinguish these terms by referring to the $I(^2P_{3/2}) + I^- \rightarrow I_2^-$ process on the lower dissociation asymptote as recombination, while the overall reaction, including

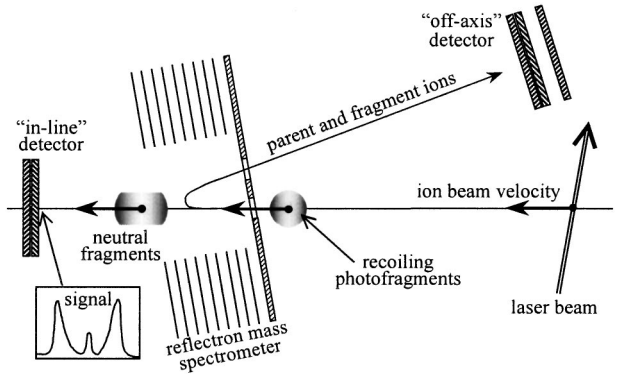

FIG. 2. Part of the experimental apparatus used for TOF analysis of neutral and ionic photofragments. It includes a reflectron mass spectrometer and two detectors. The indicated parent and fragment trajectories correspond to the measurement of translational energy release in I_2^- photodissociation.

the spin-orbit relaxation step and recombination, is referred to as caging.

Compared to caging without spin-orbit quenching,[7,10,16,66] the results reported here are more sensitive to cluster structures and solvent dynamics. Therefore, the reported caging reaction allows probing solvation with high sensitivity to details. Previously,[16] we discussed some structural effects in $I_2^-(OCS)_n$ near-UV caging dynamics, such as a steplike increase in the caging probability for $I_2^-(OCS)_{17}$, which was attributed to the completion of the first solvation shell. In this publication, we compare the results obtained with CO_2 and OCS solvents and gain additional insights into cluster structures and their role in dynamics.

II. EXPERIMENT

This section describes three types of experiments: (1) measurement of the translational energy release in the near-UV photodissociation of unsolvated I_2^-; (2) determination of the ionic product distributions in the near-UV photodissociation of the $I_2^-(CO_2)_n$ and $I_2^-(OCS)_n$ cluster ions; and (3) femtosecond pump-probe measurements of I_2^- caging in these clusters.

The tandem time-of-flight (TOF) ion beam apparatus has been described elsewhere.[41] The $I_2^-(CO_2)_n$ and $I_2^-(OCS)_n$ cluster ions are formed by attachment of slow secondary electrons to neutral clusters in an electron-impact ionized pulsed supersonic jet, followed by solvent nucleation around the negatively charged core.[3] Once the cluster ions are formed, the desired species are mass-selected in a Wiley-McLaren TOF mass spectrometer. At its spatial focus, the ion beam is crossed with a mildly focused ($\sim$2 mm) beam of pulsed laser radiation synchronized to interact only with ions of the desired mass. Other ions are deflected out of the ion beam by a pulsed electrostatic mass gate, positioned just before the crossing with the laser beam.

The remaining part of the apparatus (Fig. 2) is used for TOF analysis of neutral and ionic photofragments. It includes a second, retarding electric field (reflectron)[67,68] mass spectrometer, an off-axis microchannel plate (MCP) detector at the spatial focus of the reflectron, and an in-line MCP detector behind the reflectron. The precursor and fragment trajectories indicated in Fig. 2 pertain to the measurement of the translational energy release in I_2^- photodissociation. The fragment translational energy is uniquely defined by the photon energy (3.14 eV), the I_2^- dissociation energy (1.01 eV), and the electronic states of the fragments. For the two channels energetically accessible at 395 nm $[I(^2P_{3/2})+I^-(^1S)$ and $I^*(^2P_{1/2})+I^-(^1S)]$, we estimate 1.27 and 0.95 mm/μs fragment recoil speeds relative to the center of mass (c.m.), respectively. With the c.m. moving at 46 mm/μs relative to the lab frame (I_2^- beam velocity), the spatial distributions for the two channels are limited to two traveling concentric spheres, expanding at the above speeds.

The angular distribution of photofragments is determined by the direction of the laser polarization and the parallel nature of the $B\,^2\Sigma^+_{g,1/2} \leftarrow X\,^2\Sigma^+_{u,1/2}$ transition in I_2^-. The angular distribution indicated schematically in Fig. 2 corresponds to horizontally polarized laser radiation. The diameter of the reflectron entrance orifice is 8 mm. As the fragments pass through it, the spatial distribution is truncated, as shown in Fig. 2, for the diameter of the recoil sphere at this point is $>$9 mm (for the I^-+I^* channel).

The neutral products (I and I_2) are then separated from the parent (I_2^-) and fragment (I^-) ions by redirecting the ions toward the off-axis detector with the reflectron field. The neutral fragments pass unaffected and impact the in-line detector with the lab translational energy of about 1.5 keV for I atoms and 3 keV for I_2. The signal from this detector is amplified, digitized, averaged, and subsequently transferred to a computer. The resulting neutral fragment TOF spectrum distinguishes the I^-+I^*, I^-+I, and I_2+e^- photodestruction pathways.

In the second experiment, we measure the ionic product distributions from one-photon (395 nm) photodissociation of $I_2^-(CO_2)_n$ and $I_2^-(OCS)_n$. In this case, the reflectron voltage is set to refocus the ionic photofragments onto the off-axis detector, while the parent cluster ions, whose lab translational energy exceeds the reflectron potential barrier, impact the in-line detector. The fragment TOF signal from the off-axis detector is averaged for up to 10 000 laser shots. The resulting mass-spectra correspond to ionic fragments formed up to the entrance into the reflectron ($\sim$10 μs following the photoexcitation); subsequent fragmentation would not be detected.

For time-resolved pump-probe measurements, the reflectron voltage is adjusted to refocus two-photon (pump-probe) fragments, which are lighter than those produced by one-photon processes. Following in-cluster I_2^- dissociation by the pump photon, the probe is absorbed only if the I_2^- chromophore has recombined, and the delay dependence of the pump-probe signal reflects time-resolved caging dynamics. The typically small two-photon signals are collected by operating the off-axis detector in a single ion counting regime, by sending the amplified signal to a four-channel gated discriminator. The pump-probe signal counts are normalized to the parent cluster ion intensity, which is monitored simultaneously with the in-line detector.

For one-photon experiments, the 395 nm radiation ($\sim$7 ns pulses) is generated by frequency-doubling the output of a

Quanta-Ray PDL-1 dye laser pumped with the second harmonic of a Quanta-Ray DCR-3 Nd:YAG laser. For the ultrafast pump-probe measurements, the 790 nm radiation (1 mJ, 120 fs pulses) is generated by a femtosceond laser system[8] that includes a Coherent Mira Ti:Saphire oscillator pumped by a Coherent Nova 90 Ar^+ ion laser, and a combination of a Quantronix Series 4800 stretcher/compressor and a Ti:Saphire-based regenerative amplifier pumped by a Nd:YLF laser. For the one-color (790 nm) pump-probe measurements, the output of the ultrafast laser system is split into two identical parts (the pump and the probe), one of which passes through a computer-controlled variable delay stage. For the two-color pump-probe measurements (395 pump, 790 nm probe), the laser output is first frequency doubled and then the second harmonic light (the pump) is separated from the fundamental (the probe) with a dichroic beamsplitter. The probe beam passes through a variable delay stage and the two beams are then recombined with a similar beamsplitter and mildly focused to a 2–3 mm diameter in the ion interaction region. Background subtraction is performed using computer-controlled shutters in the pump and probe beam paths.

III. RESULTS

In this section, we first determine the fragment translational energy release in the photodissociation of unsolvated I_2^- at 395 nm and show that the photodissociation proceeds exclusively via the I^-+I^* channel. We then report the ionic product distributions in the photodissociation of $I_2^-(CO_2)_n$ and $I_2^-(OCS)_n$ clusters at the same wavelength. These distributions indicate that in clusters with $n \geqslant 7$ (for CO_2) and $n \geqslant 9$ (for OCS), the solvated chromophore dissociates via both spin-orbit channels, and the spin-orbit relaxation is often followed by $I^-+I(^2P_{3/2}) \rightarrow I_2^-$ recombination. Finally, we report the results of ultrafast pump-probe measurements, which indicate a picosecond rate of the spin-orbit relaxation and recombination.

A. Photofragment translational energy in 395 nm photodissociation of I_2^-

Figure 3 shows neutral fragment TOF spectra obtained in 395 nm photodestruction of unsolvated I_2^- with the laser polarization (a) parallel and (b) perpendicular to the flight axis *z*-fragment. The TOF distributions reflect the *z*-projections of the *z*-fragment c.m. velocity distributions, truncated at the entrance into the reflectron (see Fig. 2). The absolute kinetic energy scale is calibrated using similar TOF spectra obtained at 790 nm, where only the $I^-+I(^2P_{3/2})$ channel is open and the recoil speed is known. Using this calibration, the relative arrival times are converted into the *z*-component of fragment c.m. translational energy, indicated by the top axis in Fig. 3. The wings of the TOF distributions correspond to I fragments produced via the $I^-+I^*(^2P_{1/2})$ channel, while the central peak corresponds to nonrecoiling I_2 formed by electron photodetachment from I_2^-. No products energetically corresponding to the $I^-+I(^2P_{3/2})$ channel are observed. Thus, I_2^- photodissociation at 395 nm proceeds exclusively via the spin-orbit excited channel.

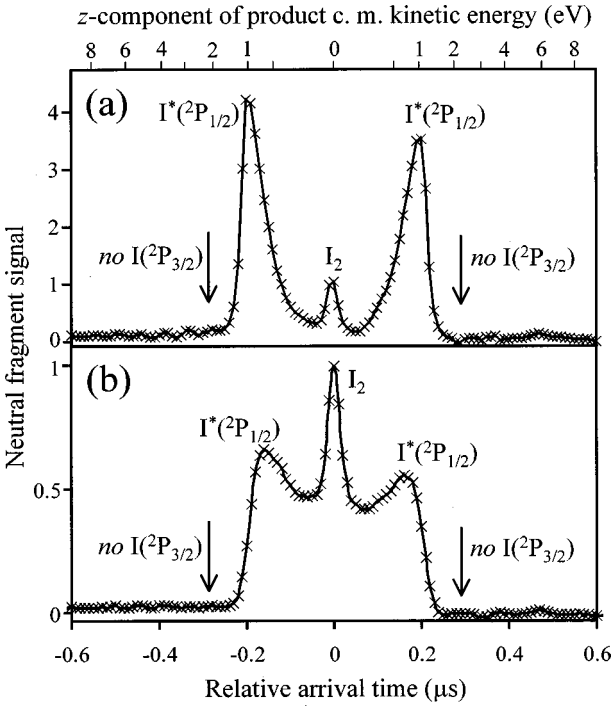

FIG. 3. Neutral photofragment TOF spectra obtained in 395 nm photodestruction of I_2^- with the laser polarization (a) parallel and (b) perpendicular to the flight axis (*z*). The fragment spatial distributions are truncated at the entrance into the reflectron (see Fig. 2). Top axis is the *z*-component of fragment c.m. translational energy.

Comparison of the TOF spectra in Figs. 3(a) and 3(b) indicates that the recoil of I^-+I^* photofragments is polarized predominantly along the laser polarization axis. It is only because of the truncation of the fragment spatial distribution at the reflectron entrance that we partially resolve the I* and I_2 channels in Fig. 3(b). (Without the truncation, the I* distribution would peak at $t=0$, similar to the I_2 channel.) The angular anisotropy thus indicates a parallel nature of the underlying transition. Indeed, the $B\,^2\Sigma^+_{g,1/2} \leftarrow X\,^2\Sigma^+_{u,1/2}$ transition dipole moment in I_2^- is parallel to the internuclear axis in both Hund's cases (a) and (c), in accord with the observations.

B. Photofragment distributions and channel branching ratios in $I_2^-(CO_2)_n$ and $I_2^-(OCS)_n$ photodissociation at 395 nm

Within clusters, I_2^- photodissociation at 395 nm is observed, in general, on both $I^-+I(^2P_{1/2,3/2})$ asymptotes. In addition, we observe I_2^- caging, which must involve $I(^2P_{1/2} \rightarrow {}^2P_{3/2})$ relaxation. Thus, three classes of photofragments are observed in the photodissociation of $I_2^-(CO_2)_n$ and $I_2^-(OCS)_n$: the uncaged fragments formed via both $I^-+I(^2P_{1/2,3/2})$ channels (A and B), and the caged products (channel C).

Figure 4 shows a typical ion fragment mass spectrum recorded in the photodissociation of $I_2^-(CO_2)_{13}$ at 395 nm. The spectrum reveals a bimodal distribution of uncaged products [$I^-(CO_2)_{3-6}$ and $I^-(CO_2)_{6-9}$], as well as a single modal distribution of caged products [$I_2^-(CO_2)_{0-3}$]. In the caged channel, 10–13 solvent molecules are lost by the clus-

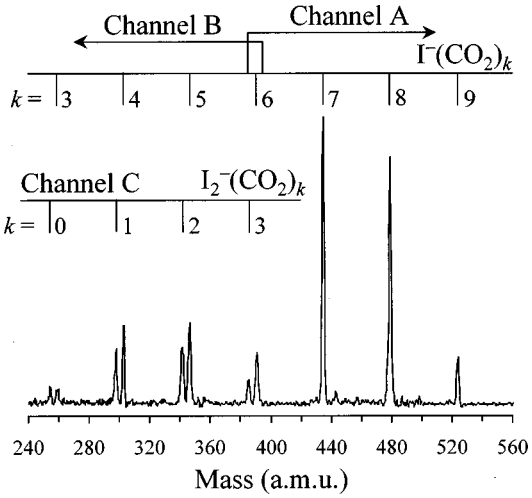

FIG. 4. Representative ion fragment mass spectrum obtained in 395 nm photodissociation of $I_2^-(CO_2)_{13}$.

ter in the caging process. Since the evaporation of each CO_2 molecule dissipates (on average) ~0.25 eV,[5,10] and given the 3.14 eV energy of 395 nm photons, the number of CO_2 molecules lost is energetically consistent with complete relaxation of the chromophore following its recombination. Similar energetic arguments indicate that the larger uncaged products correspond to the formation of $I^*(^2P_{1/2})$ (channel A), while the smaller $I^-(CO_2)_k$ fragments correspond to the formation of $I(^2P_{3/2})$ (channel B). Figure 5 shows the ionic photofragment distributions in 395 nm photodissociation of $I_2^-(CO_2)_n$ with $n=8$, 11, 13, and 17. These distributions are obtained by integrating the peaks in the fragment mass spectra. Figure 6 depicts similar distributions obtained in 395 nm

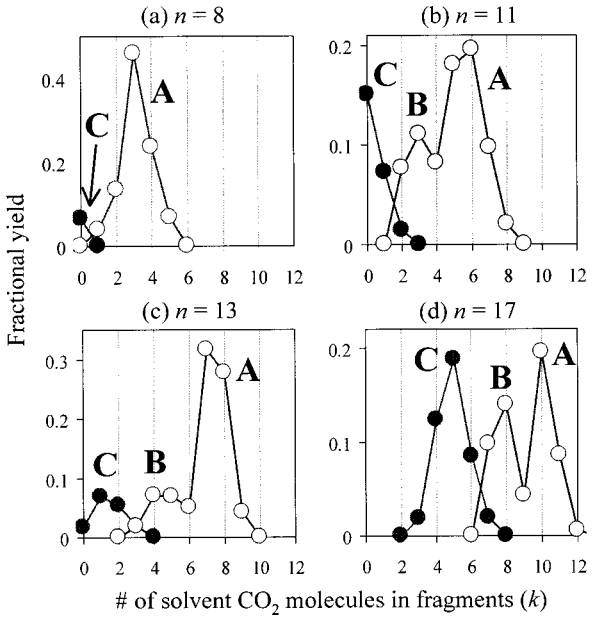

FIG. 5. Photofragment ion distributions in 395 nm photodissociation of $I_2^-(CO_2)_n$ with $n=$(a) 8, (b) 11, (c) 13, and (d) 17. The fractional fragment populations are obtained by integrating the corresponding peaks in fragment mass spectra. Filled circles indicate caged $I_2^-(CO_2)_k$ products, open circles correspond to uncaged $I^-(CO_2)_k$ fragments. A, B, and C label the corresponding reaction channels, as defined in Sec. I.

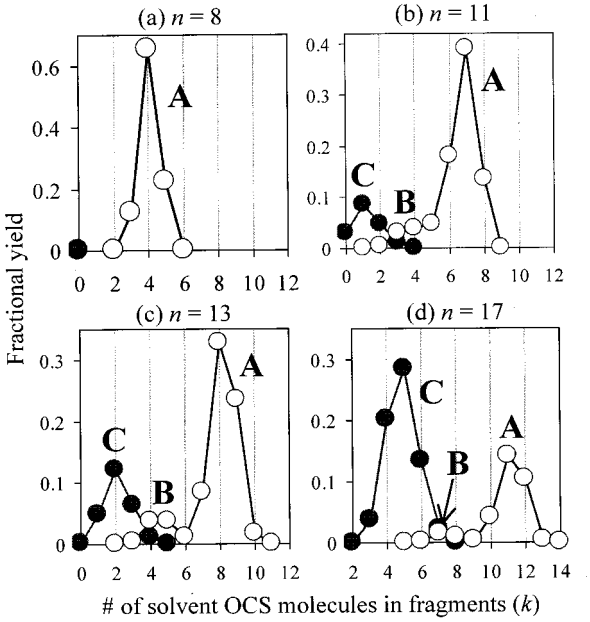

FIG. 6. Photofragment ion distributions in 395 nm photodissociation of $I_2^-(OCS)_n$ with $n=$(a) 8, (b) 11, (c) 13, and (d) 17. The fractional fragment populations are obtained by integrating the corresponding peaks in fragment mass spectra. Filled circles indicate caged $I_2^-(OCS)_k$ products, open circles correspond to uncaged $I^-(OCS)_k$ fragments. A, B, and C label the corresponding reaction channels, as defined in Sec. I.

photodissociation of $I_2^-(OCS)_n$ with the same values of n. The filled circles in Figs. 5 and 6 correspond to the caged products (channel C), while the open circles correspond to the uncaged fragments (channels A and B).

We obtained the photofragment distributions in the near-UV photodissociation of I_2^- in clusters of all sizes up to $n=19$ and 26 for the CO_2 and OCS solvents, respectively. For both solvents, the bimodal distribution of uncaged products first emerges at $n\approx10$. However, it is impossible to pinpoint the exact onset of channel B because of the overlap (in terms of k) with more intense channel A. By comparing Figs. 5 and 6, we note that the channel B parts of the uncaged product distributions are generally larger for $I_2^-(CO_2)_n$ than for $I_2^-(OCS)_n$. We also note that the relative channel intensities depend sensitively not only on the solvent, but also on the parent cluster size. In another distinction between the CO_2 and OCS solvents, the separation between the two maxima in bimodal k-distributions of uncaged products is $\Delta k=2-3$ for $I_2^-(CO_2)_n$ (Fig. 5), while it is $\Delta k\approx4$ for $I_2^-(OCS)_n$ (Fig. 6). The latter value, $\Delta k\approx4$, is more consistent energetically with statistical solvent evaporation. The smaller Δk splitting between channels A and B in the case of $I_2^-(CO_2)_n$ must be attributed to a larger (by several tenths of eV) kinetic energy release in channel B with the CO_2 solvent.

We analyze the photofragment distributions by reducing them to integrated channel branching ratios. If Y_A, Y_B, and Y_C are the total yields of respective channels, then the caging probability is defined as

$$P_{cag}=Y_C/(Y_A+Y_B+Y_C). \quad (1)$$

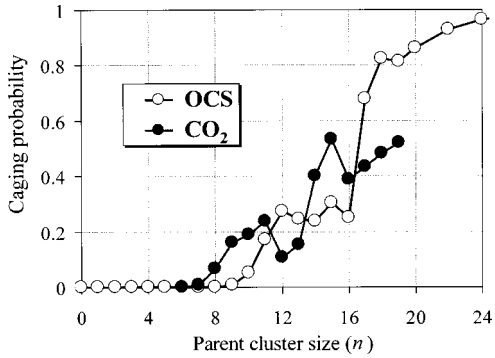

FIG. 7. The caging probabilities [$P_{cag}(n)$ according to Eq. (1)] for $I_2^-(OCS)_n$ and $I_2^-(CO_2)_n$ clusters following 395 nm photoexcitation.

The 395 nm caging probabilities for $I_2^-(CO_2)_n$ and $I_2^-(OCS)_n$, as defined by Eq. (1), are plotted versus n in Fig. 7. Note that both cluster types exhibit deviations from the monotonic behavior of $P_{cag}(n)$ in the range of $n=11-17$. This range corresponds to the $I_2^-(CO_2)_n$ and $I_2^-(OCS)_n$ clusters with approximately half-filled to complete first solvent shells.[16,39,69]

The probability of $I^*(^2P_{1/2}) \rightarrow I(^2P_{3/2})$ spin-orbit quenching is given by

$$P_{quen}=(Y_B+Y_C)/(Y_A+Y_B+Y_C). \quad (2)$$

The third important ratio describes the $I^-+I(^2P_{3/2})$ asymptote dynamics following the quenching transition. We define the probability of recombination once on the $I^-+I(^2P_{3/2})$ asymptote [referred to as the $I^-+I(^2P_{3/2})$ recombination probability] as

$$P_{rec}=Y_C/(Y_B+Y_C). \quad (3)$$

Note that $P_{cag}=P_{quen}\times P_{rec}$, as P_{cag} corresponds to the overall caging reaction probability, while P_{quen} and P_{rec} describe the two sequential steps.

Calculating the overall caging probability using Eq. (1) does not require resolving the two uncaged channels A and B; it is sufficient to resolve the caged (C) and uncaged (A+B) products. To the contrary, definitions (2) and (3) require resolving the contributions of channels A and B, which is only partially achieved in the experiment (see Figs. 5 and 6). We estimated Y_A and Y_B by fitting the bimodal uncaged distributions with a sum of two Gaussian functions, one for each channel A and B. Because the choice of the functional form for these fits is quite arbitrary, this approach leads to significant error bars and warrants caution in interpreting the results. Thus obtained values of Y_A and Y_B were used to calculate the probabilities of quenching [$P_{quen}(n)$] and $I^-+I(^2P_{3/2})$ recombination [$P_{rec}(n)$], plotted in Figs. 8(a) and 8(b), respectively.

C. Ultrafast dynamics of spin-orbit relaxation and recombination

The recombination of the chromophore revives the cluster's ability to absorb 790 nm light, and thus provides a way to observe caging in real time by monitoring the delay dependent appearance of two-photon (pump-probe) products.

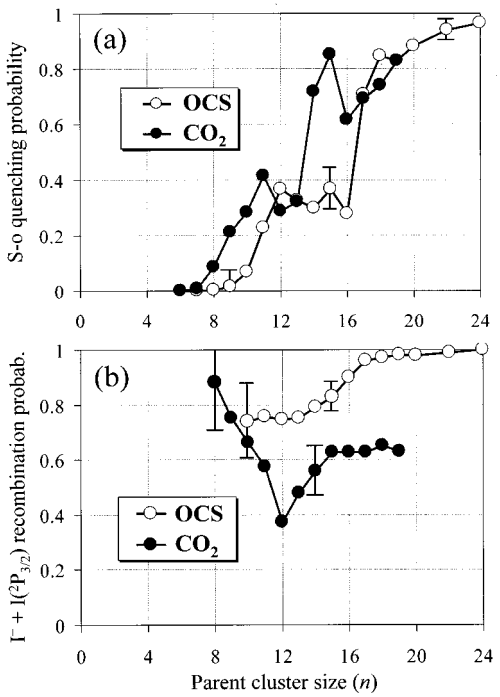

FIG. 8. (a) Spin-orbit quenching probability [$P_{quen}(n)$ defined by Eq. (2)] and (b) $I^-+I(^2P_{3/2})$ recombination probability [$P_{rec}(n)$ defined by Eq. (3)] for $I_2^-(OCS)_n$ and $I_2^-(CO_2)_n$ clusters following photoexcitation at 395 nm. The channel A and B contributions into bimodal distributions of uncaged fragments were resolved by fitting the experimental A+B distributions with a sum of two Gaussian functions, one for each channel. The estimated error bars vary with the cluster size, as indicated by selected examples in the figure.

Previous measurements using 720–790 nm excitation revealed picosecond time scales of direct (without spin-orbit quenching) caging in $I_2^-(CO_2)_n$ and $I_2^-(OCS)_n$ cluster ions.[5,7,14] Here, we investigate the time-resolved dynamics of I_2^- caging involving spin-orbit quenching of I. These dynamics reflect the cumulative time scales of the quenching and recombination processes.

The absorption recovery curves for two clusters, $I_2^-(OCS)_{17}$ and $I_2^-(OCS)_{24}$, obtained in the 395 nm pump–790 nm probe measurements are shown in Fig. 9(a). The 395 nm $B\,^2\Sigma^+_{g,1/2} \leftarrow X\,^2\Sigma^+_{u,1/2}$ transition pumped in these experiments is the same as in Secs. III A and III B. The 790 nm photon probes either the $A'\,^2\Pi_{g,1/2} \leftarrow X\,^2\Sigma^+_{u,1/2}$ transition (short arrow in Fig. 1) or the $a\,^2\Pi_{u,3/2} \leftarrow A\,^2\Pi_{g,3/2}$ transition originating from the first electronically excited I_2^- state.[5] As seen in Fig. 6(d), the photodissociation of $I_2^-(OCS)_{17}$ by the 395 nm pump yields primarily caged $I_2^-(OCS)_{4-6}$ and uncaged $I^-(OCS)_{11-12}$ one-photon products. Subsequent dissociation of the caged fragments by 790 nm probe photons at long delay yields primarily $I_2^-(OCS)_{0-1}$ and $I^-(OCS)_{2-4}$. The photodissociation of $I_2^-(OCS)_{24}$ at 395 nm results in the dominant $I_2^-(OCS)_{10-12}$ fragments, whose subsequent dissociation at 790 nm gives rise to caged $I_2^-(OCS)_{4-6}$ products accounting for more than 80% of the total fragmentation yield. The absorption recovery curves shown in Fig. 9(a) were obtained by combining signals in the most intense two-photon (395+790 nm) channels: $I_2^-(OCS)$ and $I^-(OCS)_3$ for the $I_2^-(OCS)_{17}$ parent ion and $I_2^-(OCS)_{4-6}$ for $I_2^-(OCS)_{24}$.

For $I_2^-(OCS)_{24}$, the initial rise in absorption recovery occurs on a time scale of ~2 ps, similar to the period of solvent-induced coherent $I\cdot\cdot I^-$ motion observed following 720–790 nm excitation.[5–7,14] In the smaller $I_2^-(OCS)_{17}$ cluster, the recovery is slower, similar to the 720–790 nm results for smaller clusters. To emphasize this analogy, Fig. 9(b) shows the absorption recovery curves for $I_2^-(OCS)_7$ and $I_2^-(OCS)_{17}$, obtained in 790 nm same-color pump-probe experiments. The precursor cluster sizes in Figs. 9(a) and 9(b) are purposefully different, as they were selected for the similarity of respective caging time scales. (Qualitatively, adding extra solvent molecules counterbalances the effect of doubling the energy pumped into the cluster at 395 nm, as compared to 790 nm.) In $I_2^-(OCS)_{17}$, the short-delay dynamics in Fig. 9(b) are dominated by a 2 ps bump characteristic of coherent $I\cdot\cdot I^-$ motion within the cluster, whereas in the smaller $I_2^-(OCS)_7$ cluster, the dynamics is slower and the 2 ps coherence bump does not appear.

The fast (~2 ps) rise in absorption recovery observed following 790 nm excitation of $I_2^-(OCS)_{17}$ [Fig. 9(b)] is attributed to initial recombination of the I and I^- fragments. The 2 ps time scale corresponds, therefore, to the period of pseudovibrational $I\cdot\cdot I^-$ motion in the system excited above its dissociation threshold but constrained by the solvent. The longer time scale dynamics, with the pump-probe signal leveling off after ~20 ps, reflects the internal relaxation of the caged chromophore. Despite differences in detail, time scales of I_2^- caging following 395 and 790 nm excitation [Figs. 9(a) and 9(b), respectively] are qualitatively very similar. This striking similarity indicates that the spin-orbit relaxation step implicated in Fig. 9(a), but not in Fig. 9(b), must be fast on the overall time scale of the caging reaction.

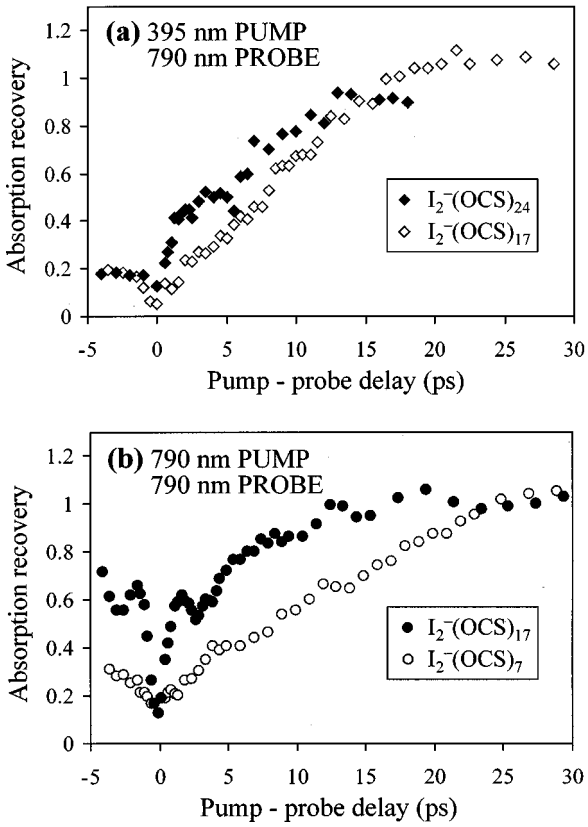

FIG. 9. Delay-dependent 790 nm absorption recoveries of indicated $I_2^-(OCS)_n$ clusters following photoexcitation at (a) 395 and (b) 790 nm. In (a), the relaxation processes leading to the caging of the I_2^- chromophore include spin-orbit relaxation of the I* fragment, while in (b) the spin-orbit relaxation step is not involved.

IV. DISCUSSION

The results presented in Sec. III provide evidence of solvent-induced spin-orbit quenching of iodine following $I_2^- \rightarrow I^- + I^*(^2P_{1/2})$ photodissociation in clusters. The evidence includes bimodal size distributions of uncaged fragments (channels A and B) and the appearance of caged products (channel C). The 395 nm caging of I_2^- is a two-step process, as indicated by chart (A)–(C): nonadiabatic coupling to an $I(^2P_{3/2})+I^-$ electronic state, followed by recombination and vibrational relaxation. For large clusters ($n>16$), the spin-orbit quenching probability approaches unity [Fig. 8(a)]. The sensitive and irregular dependence of the quenching and caging probabilities on cluster size, revealed in Figs. 8(a) and 7, respectively, is contrary to the rather smooth caging probability curves obtained in visible/near-IR photofragmentation of $I_2^-(OCS)_n$,[16] $I_2^-(CO_2)_n$,[10] and $I_2^-(N_2O)_n$ clusters.[66] The time-resolved measurements (Fig. 9) indicate very fast spin-orbit relaxation occurring on the time scale of possibly one pseudovibrational motion of the dissociated chromophore arrested by the cage. The bimodality of uncaged product distributions indicates that the spin-orbit excitation energy of iodine is transferred to the solvent cage. In addition to the observed caging, this is an indication that spin-orbit relaxation of I* occurs before the I^- and I fragments separate irreversibly.

We rule out that the appearance of spin-orbit relaxed products is due primarily to the photoexcitation of solvent-induced admixtures of I_2^- electronic states correlating with different spin-orbit asymptotes. Even at its maximum near 750 nm, the absolute cross section for excitation of the brightest state correlating with $I^-+I(^2P_{3/2})$, the A' state, is much smaller than that of the $B\leftarrow X$ transition at 395 nm. Therefore, we expect the role of short-range state mixing to be negligible, and the coupling of the $I^-+I^*(^2P_{1/2})$ and $I^-+I(^2P_{3/2})$ asymptotes to take place at large internuclear separations where the solvent-induced perturbation of the electronic structure is most significant.

At large $I\cdot\cdot I^-$ separations, the spin-orbit relaxation can involve either the I* interacting with the solvent (while the I^- acts as a spectator) or the dissociative $I^-\cdot\cdot I^*$ system as a whole, interacting with the solvent. In the former perspective, the quenching can occur either by photon emission (e.g., via the forbidden $^2P_{1/2}\rightarrow{}^2P_{3/2}$ transition in iodine),[70] or by (near-) resonant energy transfer to internal degrees of freedom of the solvent. In the $(I^-\cdot\cdot I^*)\cdot X$ system (where X denotes an ensemble of CO_2 or OCS solvent molecules), solvent-induced curve crossings and electron transfer may contribute to a relaxation mechanism.

A. Radiative relaxation

The radiative mechanism is ruled out because of the >100 ms lifetime of $I^*(^2P_{1/2})$.[71–73] The $I^*(^2P_{1/2})$

$\rightarrow I(^2P_{3/2})$ transition is electric dipole forbidden, but magnetic dipole and electric quadrupole allowed.[70] Its oscillator strength may be increased by interaction with the solvent, which lifts the parity restriction on the electric dipole radiation.[74] However, the collisional decrease in radiative lifetime observed with various colliders (Ar, Xe, SF_6) spans less than one order of magnitude for pressures up to 1 atm.[73,75] In rare gas matrices, the environment more relevant to clusters, the lifetime of $I^*(^2P_{1/2})$ decreases only to 1–5 ms.[76–78] These lifetimes are inconsistent with the picosecond time scale of spin-orbit relaxation observed in our experiments.

Additionally, photon emission by either I* or $I^-\cdot\cdot I^*$ must be ruled out of the basis of observed solvent evaporation energetics. The emission of a photon constitutes an energy loss without solvent evaporation, inconsistent with the experiment. First, the caged fragments formed with the mediation of radiative decay would lose fewer solvent molecules, compared to those formed without photon emission, because of the reduced energy available for evaporation. For large n, the average number of solvent molecules lost by caged fragments asymptotically approaches $\langle n-k\rangle \approx 12$, which is consistent with evaporative dissipation of the 3.14 eV photon energy ($\sim$0.25 eV per solvent molecule, on average). Second, the observed bimodal distributions of uncaged fragments result from the spin-orbit excitation energy being transferred to the solvent cage in channel B and then dissipated by solvent loss. If the spin-orbit excitation were quenched by photon emission, this energy would not become available for evaporation.

B. Spin-orbit quenching by energy transfer from I* to solvent

The quenching of electronically excited halogen atoms in collisions has been studied extensively, and its efficiency is known to vary greatly depending on the collision partners.[79] The probabilities of spin-orbit relaxation of I* on a single collision with rare gas atoms are less than 10^{-8}, increasing by orders of magnitude for some molecular colliders.[79] The largest I* quenching probability ($\sim 5\times 10^{-2}$ per collision) is observed for O_2,[79] and is due to the near resonance between the $^2P_{1/2}\rightarrow{}^2P_{3/2}$ and $^1\Delta_g\leftarrow{}^3\Sigma_g^-$ transitions in I and O_2, respectively. Relatively fast quenching rates were observed by Hofmann and Leone in collisions of I* with halogen molecules,[80] but the relaxation proceeds by a reactive mechanism, which is not applicable to the present study. In direct relation to the present work, the quenching probability of $I^*(^2P_{1/2})$ by CO_2 was measured to be 5.7×10^{-7} per collision.[79] This probability cannot explain the efficiency of spin-orbit relaxation in our experiment. Remarkably, the quenching by CO_2 is much more efficient for $Br^*(^2P_{1/2})$ ($\sim 10^{-1}$ per collision), due to the near resonant electronic to vibrational ($E\rightarrow V$) energy transfer.[81] Hariri and Wittig identified the (101) vibrational state of CO_2, which is nearly resonant with $Br^*(^2P_{1/2})$, as a major product channel in this energy transfer reaction.[81] By studying various colliders, they also concluded that the quenching process becomes less efficient with increasing number of vibrational quanta needed to achieve a near resonance. This conclusion is consistent with carbon dioxide's inefficiency in quenching I*, whose spin-orbit excitation energy is more than twice as large as that of Br*.

Since I* quenching by $E\rightarrow V$ energy transfer to the solvent cage is inefficient, a different mechanism must be invoked. Assuming that the relaxation involves only the $I^*\cdot X$ system, a (near) resonance or curve crossing between $I^*\cdot X$ and $I\cdot X$ quantum states is generally needed. In the case of Br^*/CO_2, such resonance is between the $Br^*(^2P_{1/2})\cdot CO_2(000)$ and $Br(^2P_{3/2})\cdot CO_2(101)$ electronic-vibrational states. In $I\cdot CO_2$ and I·OCS, in the absence of suitable electronic-vibrational resonances (see above), we are left to explore the possibility of electronic curve crossings. Because the $I\cdot CO_2$ and I·OCS van der Waals interactions are relatively weak, no crossings exist between the $I^*\cdot X$ and $I\cdot X$ electronic states, at least at energies accessible in these experiments. The absence of crossings was confirmed by *ab initio* calculations on both $I\cdot CO_2$ and I·OCS.[64,82,83]

C. Spin-orbit quenching by solvent asymmetry mediated electron transfer

So far, we considered the I^- fragment as a mere spectator, with the quenching transitions involving only the quantum states of I* and the solvent. This strategy failed in interpreting the results. As another clue, I* quenching on a picosecond time scale has not been observed in neutral environments. Therefore, the proximity of the I^- fragment and the perturbed electronic structure of the dissociative $I^-\cdot\cdot I^*$ system are likely to be key to understanding the relaxation mechanism.

As discussed by Parson and co-workers in the companion paper,[65] solvation effects involving the anion can compensate for the energy gap between the two spin-orbit asymptotes. Because of the substantial binding energy of OCS and CO_2 to the cluster ($\sim$0.2 eV per molecule),[5,10,16] the relative state energies are greatly affected by asymmetries of the solvent and charge distributions. Consider the example in Fig. 10. For the unsolvated $I\cdot\cdot I^-$ system (left), the $I^-+I(^2P_{3/2})$ and $I^-+I^*(^2P_{1/2})$ electronic states are separated by 0.93 eV. These states are degenerate with respect to switching the fragment positions (i.e., I^-+I versus $I+I^-$, and I^-+I^* versus I^*+I^-). This degeneracy is lifted by asymmetric solvation of the fragment pair (Fig. 10, right). If the charge is localized at the more solvated end of the cluster, the corresponding state energy is lowered significantly. On the other hand, if the charge is localized on the least solvated end, the energy is affected less. If the differential solvation energy ($\Delta\Phi$) is about 0.93 eV, the $X\cdot I^-\cdot\cdot I^*$ and $X\cdot I\cdot\cdot I^-$ states come into resonance, and a rapid spin-orbit quenching transition is possible by electron transfer from I^- to I*. Following the $X\cdot I^-\cdot\cdot I^*\rightarrow X\cdot I\cdot\cdot I^-$ transition, the electrostatic attraction between the solvent and I^- will tend to reverse the dissociation trajectory toward I_2^- recombination. In the companion paper,[65] Delaney *et al.* explore this mechanism by molecular dynamics simulations, and achieve good agreement with our experimental results.

Figure 10 is intended as a qualitative illustration and it oversimplifies the energetics and dynamics of quenching. The number and configuration of solvent CO_2 molecules are

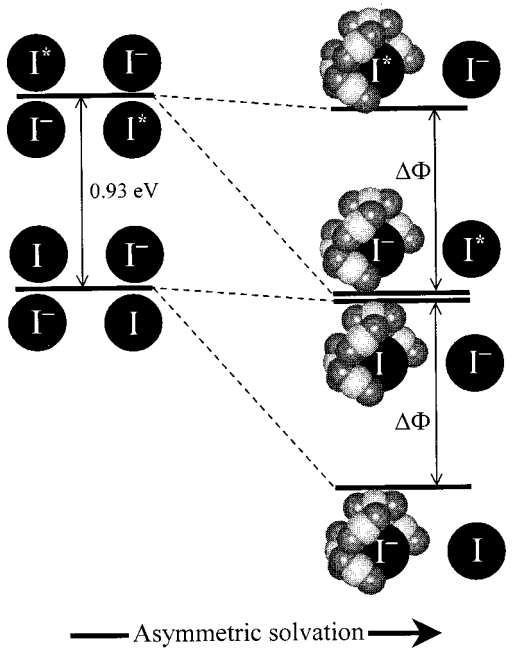

FIG. 10. An energy diagram illustrating the mechanism of spin-orbit relaxation by solvent mediated electron transfer from I^- to I* in an asymmetrically solvated cluster. The required resonance between the $X \cdot I^- \cdot \cdot I^*$ and $X \cdot I \cdot \cdot I^-$ electronic states occurs when the differential solvation energy ($\Delta\Phi$) is equal to the spin-orbit energy gap in iodine (0.93 eV).

chosen arbitrarily to satisfy $\Delta\Phi \approx 0.93$ eV. Of course, resonances between different electron-transfer states are possible with a broad range of solvent configurations. In some cases, such as when the number of solvent molecules in the parent cluster is close to a complete solvent shell, dissociation trajectories start out from nearly symmetric solvent configurations. However, as the cluster breaks up and the charge localizes on one of the fragments, the initial symmetry is destroyed. As long as the number of solvent molecules in the cluster is sufficient, the required asymmetry can be achieved at some $I \cdot \cdot I^-$ separation, as the solvent gravitates toward the charge.

Given the solvent binding energy of ~0.2 eV per CO_2 or OCS molecule, at least 4–5 solvent molecules are needed to possibly achieve the solvent asymmetry ($\Delta\Phi \approx 0.93$ eV) required for an $X \cdot I^- \cdot \cdot I^* - X \cdot I \cdot \cdot I^-$ resonance. This minimum number must be increased to account for solvent loss before the charge becomes localized and solvent rearrangement takes place. Qualitatively, we expect at least $n \approx 7$ as a low limit for quenching transitions. Theoretical simulations by Delaney *et al.* indicate an onset of quenching in $I_2^-(CO_2)_n$ at $n=8$.[65] In the experiment, we see rather sharp onsets of quenching at $n=7$ for $I_2^-(CO_2)_n$ and $n \approx 9$ for $I_2^-(OCS)_n$ [see Fig. 8(a)], in good agreement with the above analysis. Note that were the spin-orbit relaxation occurring by $E \rightarrow V$ energy transfer from I* to the solvent, no sharp threshold would be expected. Therefore, the observed thresholds are another experimental indication in favor of the electron transfer mechanism.

Despite the difficulties in determining the onset (in terms of n) of the $I^- + I(^2P_{3/2})$ channel (channel B), it is apparent that it does not precede the opening of the caged channel. As seen in Fig. 5(a), the caged channel of $I_2^-(CO_2)_n$ photofragmentation is already open at $n=8$, but a bimodal $I^-(CO_2)_k$ distribution is not yet evident. Despite the possible channel A and B overlap, from the $I^-(CO_2)_k$ distribution maximum at $k=3$ (corresponding to channel A), we expect a contribution to channel B at $k=0$, but no I^- fragments are observed. Thus, following the spin-orbit relaxation step, we do not observe a preference for dissociation on the ground spin-orbit asymptote, even in the smallest clusters in which the quenching is possible.

This observation is contrary to the results obtained when the A' state of I_2^- is photoexcited, in which case the dynamics on the lower spin-orbit asymptote in small clusters naturally favors dissociation rather than recombination.[7,10,16,66] In fact, I_2^- dissociation to $I^- + I(^2P_{3/2})$ is the only 790 nm channel observed for $n<4$ in $I_2^-(CO_2)_n$,[7] and $n<3$ in $I_2^-(OCS)_n$.[16] At 395 nm, there is no preference for $I^- + I(^2P_{3/2})$ dissociation because of the restrictions imposed by the spin-orbit relaxation step. As we discussed, the quenching can occur only if the number of solvent molecules in the cluster is sufficiently large, which by itself favors recombination. Additionally, following the electron transfer/quenching step, the charge in the $X \cdot I \cdot \cdot I^-$ state localizes on the escaping fragment (see Fig. 10), which experiences a backward pull from the rest of the cluster. Thus, solvent configurations that are prerequisite for quenching are also favorable for recombination.

Contrarily, if the electron transfer fails during the initial fragment separation in the $X \cdot I^- \cdot \cdot I^*$ state, the electrostatic force acting on the escaping neutral fragment is weak, and subsequent dynamics favors cage escape. Consequently, the dynamical window for spin-orbit quenching may be quite narrow, limited to initial fragment separation, which is consistent with the fast time scale of caging observed experimentally. Since the quenching step does not add extra time to that needed for fragment separation and subsequent recombination, similar caging time scales are to be expected following the dissociation to $I^- + I^*(^2P_{1/2})$ and $I^- + I(^2P_{3/2})$, in accord with the remarkably similar experimental dynamics shown in Figs. 9(a) and 9(b), respectively.

D. Structural implications

The resonance condition for spin-orbit relaxation by solvent asymmetry mediated electron transfer is very sensitive to instantaneous solvent configurations.[65] Therefore, the caging reaction involving spin-orbit relaxation is a sensitive probe of solvation. Previously, we discussed some structural effects in $I_2^-(OCS)_n$ caging dynamics, such as the step like increase in the caging probability for $I_2^-(OCS)_{17}$ (see Fig. 7).[16] This increase was attributed to the completion of the first solvation shell in $I_2^-(OCS)_n$ at $n=17$. At present, comparison of the $I_2^-(OCS)_n$ and $I_2^-(CO_2)_n$ results yields additional insights into the role of structure in dynamics.

First, the most prominent feature of the $I_2^-(OCS)_n$ caging probability curve in Fig. 7, besides the almost threefold increase at $n=17$, is the plateau at $n=12-16$. No such plateau is observed for $I_2^-(CO_2)_n$, for which caging in the same cluster size range exhibits seemingly erratic behavior. It is re-

vealing that the $I_2^-(OCS)_n$ plateau consists of exactly five cluster sizes. Recent calculations predicted that the first OCS solvent shell around I_2^- consists of three five-membered OCS rings plus two end molecules ''capping'' the cluster.[16] The plateau corresponds to the formation of the third solvent ring around the chromophore. Similar calculations indicated qualitatively different $I_2^-(CO_2)_n$ structures, which are not based on solvent rings.[39,69] Accordingly, we observe no caging probability plateau for $I_2^-(CO_2)_n$.

Second, as seen Figs. 8(a) and 7, the onset of spin-orbit relaxation and caging is observed in smaller $I_2^-(CO_2)_n$ clusters, compared to $I_2^-(OCS)_n$ ($n=7$ versus 9). This difference cannot be explained by kinematics or energetics. First, OCS is heavier than CO_2, and therefore fewer OCS molecules are kinematically equivalent to any number of CO_2's. Second, the CO_2 and OCS binding energies to I_2^- clusters are very similar.[5,10,16] Moreover, at 790 nm, caging onsets slightly earlier in OCS than in CO_2.[16] Because the spin-orbit relaxation is more sensitive to cluster structures than the ground asymptote dynamics, we suggest a structural explanation for the 395 nm result. Since the predicted $I_2^-(OCS)_n$ structures are more symmetric compared to $I_2^-(CO_2)_n$ (solvent rings versus no rings),[16] the degree of differential solvation needed for quenching ($\Delta\Phi\approx 0.93$ eV) requires more solvent reorganization in OCS and is therefore harder to achieve.

Third, for both $I_2^-(OCS)_n$ and $I_2^-(CO_2)_n$, the caging probabilities are rather smooth and monotonic outside the range of $n=11-17$ (see Fig. 7). Only in this mid-size range, where the second half of the first solvent shell is believed to be constructed,[16,39,69] the caging behavior deviates from the intuitively expected monotonic rise, such as the 790 nm trend.[7,10,16,66] For smaller clusters, the too few available solvent molecules restrict the quenching trajectories because of the limited number of the extremely asymmetric solvent configurations that satisfy $\Delta\Phi\approx 0.93$ eV. Each additional solvent molecule alleviates this constraint, increasing the quenching and caging probabilities. In the mid-size range ($n=11-17$), the number of solvents is already quite large, so that the required degree of differential solvation is achieved without imposing strict dynamical restrictions. In this size range, the details of cluster structure, not the mere number of solvent molecules, become critical in determining the quenching and caging probabilities. This trend continues until the first solvent shell is filled at $n=16$ [$I_2^-(CO_2)_n$] or 17 [$I_2^-(OCS)_n$]. From there on, additional solvent molecules do not introduce significant structural changes, and the dynamics revert to a monotonic increase in caging probability with n.

Fourth, we observe that in large cluster ($n>16$), the spin-orbit quenching probabilities are similar for $I_2^-(CO_2)_n$ and $I_2^-(OCS)_n$ [see Fig. 8(a)]. However, following the quenching transition, the probability of $I^-+I(^2P_{3/2})$ recombination in OCS approaches unity for $n>16$, while in CO_2 ($n>16$) nearly 40% of quenched trajectories lead to $I^-+I(^2P_{3/2})$ dissociation [Fig. 8(b)]. This difference may be due to several factors. (1) One factor may be a kinematic effect, since OCS is heavier than CO_2. However, if this were the dominant factor, a similar effect would be expected at 790 nm, contrary to the observations.[16] (2) In the quenched $X\cdot I\cdot\cdot I^-$ state (Fig. 10), the charge-dipole interactions of OCS with the escaping I^- are more effective in pulling back the I^- fragment, compared to the shorter-range charge-quadrupole interactions involving CO_2. (3) We cannot rule out that in $I_2^-(OCS)_n$, the electron transfer transitions occur at shorter $I\cdot\cdot I^-$ distances, compared to $I_2^-(CO_2)_n$, which may also favor subsequent recombination.

Finally, we observe a consistent distinction between the CO_2 and OCS solvents in bimodal size distributions of uncaged products. As seen in Fig. 6, for $I_2^-(OCS)_n$ the channel A and B maxima in the distributions are typically separated by about four solvent molecules ($\Delta k\approx 4$), which is consistent with solvent evaporation energetics. However, substantially smaller separations, ($\Delta k=2-3$), are observed for $I_2^-(CO_2)_n$ (Fig. 5), although the evaporation energetics are known to be similar. The reduction in Δk can be due to increased translational energy release to final products via channel B in $I_2^-(CO_2)_n$. The increase may be due to incomplete energy redistribution among the chromophore fragments and solvent in the decomposing cluster, because of the shorter, compared to $I_2^-(OCS)_n$, range of the dominant interactions (charge-quadrupole). This argument is similar to that in the previous paragraph regarding the reduced $I^-+I(^2P_{3/2})$ recombination probability [$P_{rec}(n)$] in large $I_2^-(CO_2)_n$ clusters. Note that the translational energy release in channel A would also be affected by incomplete energy redistribution, but to a lesser degree, because the I^-+I^* translational energy released in channel A is nearly two times smaller.

V. SUMMARY

In summary, the near-UV photodissociation of I_2^- in clusters leads to a new type of photofragment caging reaction that involves spin-orbit relaxation. The photoexcitation promotes the chromophore to a dissociative state correlating with $I^-+I^*(^2P_{1/2})$, which is the only dissociation channel in unsolvated I_2^-. In clusters, interaction with the solvent results in three pathways: (1) direct dissociation to $I^-+I^*(^2P_{1/2})$, leading to channel A uncaged products; (2) dissociation followed by spin-orbit quenching, leading to channel B uncaged products; (3) dissociation and spin-orbit quenching, followed by I_2^- recombination and vibrational relaxation, leading to caged products.

In large cluster ($n>16$), the probability of spin-orbit quenching approaches unity for both CO_2 and OCS solvents, although subsequent $I(^2P_{3/2})+I^-$ dynamics in the two solvents vary. The time-resolved measurements indicate that caging and (consequently) spin-orbit relaxation are fast, occurring on picosecond time scales. The quenching mechanisms involving radiative relaxation and energy transfer from I^* to the solvent fail to explain the observed reaction time scales and efficiency. Instead, the spin-orbit relaxation takes place in the solvated $I\cdot\cdot I^-$ system by electron transfer from I^- to I^*, as the electron donor fragment transforms into the ground state I atom. The 0.93 eV gap between the initial and final states in this transition is bridged by differential solvation due to solvent asymmetry.[65]

The new type of caging reaction explicitly relies on strong perturbation of the I_2^- electronic structure by the sol-

vent and is subtly sensitive to details of cluster structure and the nature of dominant interactions. The required degree of perturbation requires at least ~ 7 solvent molecules in the parent cluster, which is in agreement with the observed onset of 395 nm caging. The results are in qualitative accord with the molecular dynamics simulations of Parson and co-workers.[65]

Future experiments will focus on dynamical differences between the spin-orbit relaxation mechanisms relying on electron transfer and near-resonant energy transfer to the solvent. These experiments will be carried out on $IBr^-(CO_2)_n$ and $Br_2^-(CO_2)_n$ cluster ions. In both cases, the solvated chromophore will be dissociated via a channel yielding $Br^*(^2P_{1/2})$. The ensuing spin-orbit relaxation of Br* can proceed either via the electron transfer mechanism discussed here, or by $E \rightarrow V$ energy transfer to CO_2. According to Hariri and Wittig,[81] the $E \rightarrow V$ energy transfer mechanism is remarkably more efficient in Br^*/CO_2 ($\sim 10^{-1}$ per collision) than in I^*/CO_2, as a result of the near-resonance between the $Br^*(^2P_{1/2}) \cdot CO_2(000)$ and $Br(^2P_{3/2}) \cdot CO_2(101)$ electronic-vibrational states. Possible competition between the two mechanisms may lead to new exciting opportunities.

ACKNOWLEDGMENTS

We thank our theoretical collaborators Nicole Delaney, James Faeder, and Robert Parson for many fruitful and enthusiastic discussions and insights into the interpretation of results. This work is supported by the National Science Foundation (Grant Nos. CHE97-03486 and PHY95-12150) and the Air Force Office of Scientific Research (AASERT program).

[1] A. W. Castleman and K. H. Bowen, J. Phys. Chem. **100**, 12911 (1996).
[2] J. M. Farrar, in *Current Topics in Ion Chemistry and Physics*, edited by C. Y. Ng and I. Powis (Wiley, New York, 1992).
[3] M. A. Johnson and W. C. Lineberger, in *Techniques for the Study of Ion Molecule Reactions*, edited by J. M. Farrar and J. W. Saunders (Wiley, New York, 1988), p. 591.
[4] A. W. Castleman, Jr., in *Clusters of Atoms and Molecules*, edited by H. Haberland (Springer-Verlag, New York, 1992).
[5] J. M. Papanikolas, V. Vorsa, M. E. Nadal, P. J. Campagnola, H. K. Buchenau, and W. C. Lineberger, J. Chem. Phys. **99**, 8733 (1993).
[6] J. M. Papanikolas, V. Vorsa, M. E. Nadal, P. J. Campagnola, J. R. Gord, and W. C. Lineberger, J. Chem. Phys. **97**, 7002 (1992).
[7] V. Vorsa, S. Nandi, P. J. Campagnola, M. Larsson, and W. C. Lineberger, J. Chem. Phys. **106**, 1402 (1997).
[8] V. Vorsa, P. J. Campagnola, S. Nandi, M. Larsson, and W. C. Lineberger, J. Chem. Phys. **105**, 2298 (1996).
[9] J. M. Papanikolas, P. J. Campagnola, V. Vorsa, M. E. Nadal, H. K. Buchenau, R. Parson, and W. C. Lineberger, in *The Chemical Dynamics and Kinetics of Small Radicals*, edited by K. Liu and A. Wagner (World Scientific, Singapore, 1995), Vol. 6, p. 616.
[10] J. M. Papanikolas, J. R. Gord, N. E. Levinger, D. Ray, V. Vorsa, and W. C. Lineberger, J. Phys. Chem. **95**, 8028 (1991).
[11] D. Ray, N. E. Levinger, J. M. Papanikolas, and W. C. Lineberger, J. Chem. Phys. **91**, 6533 (1989).
[12] B. J. Greenblatt, M. T. Zanni, and D. M. Neumark, Science **276**, 1675 (1997).
[13] B. J. Greenblatt, M. T. Zanni, and D. M. Neumark, Chem. Phys. Lett. **258**, 523 (1996).
[14] A. Sanov, S. Nandi, and W. C. Lineberger, J. Chem. Phys. **108**, 5155 (1998).
[15] A. Sanov and W. C. Lineberger, Proc. SPIE **3271**, 188 (1998).
[16] S. Nandi, A. Sanov, N. Delaney, J. Faeder, R. Parson, and W. C. Lineberger, J. Phys. Chem. **102**, 8827 (1998).
[17] A. E. Johnson, N. E. Levinger, and P. F. Barbara, J. Phys. Chem. **96**, 7841 (1992).
[18] J. C. Alfano, Y. Kimura, P. K. Walhout, and P. F. Barbara, Chem. Phys. **175**, 147 (1993).
[19] D. A. V. Kliner, J. C. Alfano, and P. F. Barbara, J. Chem. Phys. **98**, 5375 (1993).
[20] P. K. Walhout, J. C. Alfano, K. A. M. Thakur, and P. F. Barbara, J. Phys. Chem. **99**, 7568 (1995).
[21] U. Banin, R. Kosloff, and S. Ruhman, Chem. Phys. **183**, 289 (1994).
[22] U. Banin and S. Ruhman, J. Chem. Phys. **98**, 4391 (1993).
[23] U. Banin and S. Ruhman, J. Chem. Phys. **99**, 9318 (1993).
[24] E. Gershgoren, U. Banin, and S. Ruhman, J. Phys. Chem. A **102**, 9 (1998).
[25] H. Yasumatsu, S. Koizumi, A. Terasaki, and T. Kondow, J. Chem. Phys. **105**, 9509 (1996).
[26] H. Yasumatsu, A. Terasaki, and T. Kondow, J. Chem. Phys. **106**, 3806 (1997).
[27] H. Yasumatsu, U. Kalmbach, S. Koizumi, A. Terasaki, and T. Kondow, Z. Phys. D **40**, 1 (1997).
[28] H. Yasumatsu, A. Terasakia, and T. Kondow, Int. J. Mass Spectrom. Ion Processes **174**, 1 (1998).
[29] F. G. Amar and L. Perera, Z. Phys. D **20**, 173 (1991).
[30] B. J. Gertner, K. Ando, R. Bianco, and J. T. Hynes, Chem. Phys. **183**, 309 (1994).
[31] R. Bianco and J. T. Hynes, J. Chem. Phys. **102**, 7864 (1995).
[32] R. Bianco and J. T. Hynes, J. Chem. Phys. **102**, 7885 (1995).
[33] I. Benjamin, P. F. Barbara, B. J. Gertner, and J. T. Hynes, J. Phys. Chem. **99**, 7557 (1995).
[34] J. M. Papanikolas, P. E. Maslen, and R. Parson, J. Chem. Phys. **102**, 2452 (1995).
[35] J. Faeder, N. Delaney, P. E. Maslen, and R. Parson, Chem. Phys. Lett. **270**, 196 (1997).
[36] J. Faeder and R. Parson, J. Chem. Phys. **108**, 3909 (1998).
[37] P. E. Maslen, J. M. Papanikolas, J. Faeder, R. Parson, and S. V. ONeil, J. Chem. Phys. **101**, 5731 (1994).
[38] B. M. Ladanyi and R. Parson, J. Chem. Phys. **107**, 9326 (1997).
[39] N. Delaney, J. Faeder, P. E. Maslen, and R. Parson, J. Phys. Chem. A **101**, 8147 (1997).
[40] R. Parson and J. Faeder, Science **276**, 1660 (1997).
[41] M. E. Nadal, P. D. Kleiber, and W. C. Lineberger, J. Chem. Phys. **105**, 504 (1996).
[42] V. S. Batista and D. F. Coker, J. Chem. Phys. **106**, 7102 (1997).
[43] B. J. Greenblatt, M. T. Zanni, and D. M. Neumark, Chem. Phys. Lett. **258**, 523 (1996).
[44] M. T. Zanni, T. R. Taylor, B. J. Greenblatt, B. Soep, and D. M. Neumark, J. Chem. Phys. **107**, 7613 (1997).
[45] J. Troe, Annu. Rev. Phys. Chem. **29**, 223 (1978).
[46] B. Otto, J. Schroeder, and J. Troe, J. Chem. Phys. **81**, 202 (1984).
[47] H. Kunz, J. G. McCaffrey, R. Schriever, and N. Schwentner, J. Chem. Phys. **94**, 1039 (1991).
[48] J. Xu, N. Schwentner, and M. Chergui, J. Chem. Phys. **101**, 7381 (1994).
[49] K. H. Godderz, N. Schwentner, and M. Chergui, J. Chem. Phys. **105**, 451 (1996).
[50] V. E. Bondybey and L. E. Brus, Adv. Chem. Phys. **41**, 269 (1980).
[51] P. S. Dardi and J. S. Dahler, J. Chem. Phys. **93**, 242 (1990).
[52] G. N. R. Tripathi, R. H. Schuler, and R. W. Fessenden, Chem. Phys. Lett. **113**, 563 (1985).
[53] X. Xu, S. Yu, R. Lingle, H. Zhu, and J. B. Hopkins, J. Chem. Phys. **95**, 2445 (1991).
[54] A. L. Harris, J. K. Brown, and C. B. Harris, Annu. Rev. Phys. Chem. **39**, 341 (1988).
[55] R. Zadoyan, Z. Li, C. C. Martens, and V. A. Apkarian, J. Chem. Phys. **101**, 6648 (1994).
[56] R. Zadoyan, Z. Li, P. Ashjian, C. C. Martens, and V. A. Apkarian, Chem. Phys. Lett. **218**, 504 (1994).
[57] Q. Liu, J. K. Wang, and A. H. Zewail, Nature (London) **364**, 427 (1993).
[58] E. D. Potter, Q. Liu, and A. H. Zewail, Chem. Phys. Lett. **200**, 605 (1992).
[59] Q. L. Liu, J. K. Wang, and A. H. Zewail, J. Phys. Chem. **99**, 11321 (1995).
[60] J. K. Wang, Q. L. Liu, and A. H. Zewail, J. Phys. Chem. **99**, 11309 (1995).
[61] E. Rabinowitch and W. C. Wood, Trans. Faraday Soc. **32**, 547 (1936).
[62] E. Rabinowitch and W. C. Wood, Trans. Faraday Soc. **32**, 1381 (1936).
[63] J. Franck and E. Rabinowitch, Trans. Faraday Soc. **30**, 120 (1934).

[64] J. Faeder, N. Delaney, P. E. Maslen, and R. Parson, Chem. Phys. **239**, 525 (1998).
[65] N. Delaney, J. Faeder, and R. Parson, J. Chem. Phys. **111**, 651 (1999), preceding paper.
[66] M. E. Nadal, Ph.D. Thesis, University of Colorado, 1996.
[67] M. L. Alexander, Ph.D. Thesis, University of Colorado, 1987.
[68] B. A. Mamyrin, V. I. Karataev, D. V. Shmikk, and V. A. Zagulin, Sov. Phys. JETP **37**, 45 (1973).
[69] J. M. Papanikolas, P. E. Maslen, and R. Parson, J. Chem. Phys. **102**, 2452 (1995).
[70] G. Herzberg, *Atomic Spectra and Atomic Structure* (Dover, New York, 1948).
[71] D. E. O'Brien and J. R. Bowen, J. Appl. Phys. **40**, 4767 (1969).
[72] F. J. Comes and S. Pionteck, Chem. Phys. Lett. **42**, 558 (1976).
[73] R. Engleman, Jr., B. A. Palmer, and S. J. Davis, J. Opt. Soc. Am. **73**, 1585 (1983).
[74] V. Y. Zalesskii and T. I. Krupenikova, Opt. Spectrosc. **30**, 439 (1971).
[75] L. S. Ershov and V. Y. Zalesskii, Sov. J. Quantum Electron. **8**, 649 (1978).
[76] M. Macler, J. P. Nicolai, and M. C. Heaven, J. Chem. Phys. **91**, 674 (1989).
[77] R. Bohling, J. Langen, and U. Schurath, Chem. Phys. **130**, 419 (1989).
[78] W. G. Lawrence and V. A. Apkarian, J. Chem. Phys. **101**, 1820 (1994).
[79] See the review by D. Husain and R. J. Donovan, in *Advances in Photochemistry*, edited by J. N. Pitts, Jr., G. S. Hammond, and W. A. Noyers, Jr. (Wiley-Interscience, New York, 1971), Vol. 8, and references therein.
[80] H. Hofmann and S. R. Leone, J. Chem. Phys. **69**, 641 (1978).
[81] A. Hariri and C. Wittig, J. Chem. Phys. **67**, 4454 (1977).
[82] A. Sanov, J. Faeder, R. Parson, and W. C. Lineberger, Chem. Phys. Lett. (submitted).
[83] D. W. Arnold, S. E. Bradforth, E. H. Kim, and D. M. Neumark, J. Chem. Phys. **102**, 3493 (1995).